Electronic Supplementary Information (ESI)

MOF-on-MOF heterojunctions derived Co_3O_4-$CoCo_2O_4$ microflowers for low-temperature catalytic oxidation

Jingwen Mao,[a] Qin Meng,[b] Zehai Xu,[a] Lusheng Xu,[a] Zheng Fan[a] and Guoliang Zhang*,[a]

[a] *Institute of Oceanic and Environmental Chemical Engineering, Center for Membrane and Water Science &Technology, State Key Lab Breeding Base of Green Chemical Synthesis Technology, Zhejiang University of Technology, Chaowang Road 18#, Hangzhou, Zhejiang 310014, China*
Tel/Fax: 86-571-88320863

[b] *College of Chemical and Biological Engineering, State Key Laboratory of Chemical Engineering, Zhejiang University, 38 Zheda Road, Hangzhou, Zhejiang 310027, China*

**Corresponding author E-mail: guoliangz@zjut.edu.cn*

Contents

1. Experimental detail

    1.1 Materials

    1.2 Methods

    1.3 Characterization

    1.4 Catalytic experiments

    1.5 Catalysis kinetics

2. Results and Discussions

1. Experimental details

1.1 Materials

All reagents were purchased commercially and used without further purification. Copper(II) nitrate trihydrate ($Cu(NO_3)_2·3H_2O$, 99%), Ferric nitrate nonahydrate ($Fe(NO_3)_3·9H_2O$, 99%), Aluminum nitrate nonahydrate ($Al(NO_3)_3·9H_2O$, 99%), zirconium tetrachloride ($ZrCl_4$, 99%) and cobalt(II) acetate tetrahydrate ($Co(OAc)_2·4H_2O$, 99%) in A.R. grade was purchased from Sinopharm Chemical Reagent Co., Ltd., China. 1,4-dicarboxybenzene (H_2BDC, 99%) and 2-methylimidazole (2-MeIM, 98%) were purchased from Aladdin Industrial Corporation. N,N-dimethylformamide (DMF, ≥99.5%), methanol (MeOH, ≥99.5%) and absolute ethanol (EtOH, ≥99.7%) in A.R. grade were purchased from Shanghai Lingfeng Chemical Reagent Co., Ltd, China. All experiment solutions were prepared from deionized water manufactured by a self-made RO-EDI system.

1.2 Methods

Synthesis of layered stacked CuBDC. CuBDC was synthesized by a conventional solution method. The solution of $Cu(NO_3)_2·3H_2O$ in 14 ml DMF and H_2BDC in 14 ml DMF were mixed and placed in a water bath at 323 K for 3 days. After cooling down, the resulting blue powders were isolated under centrifugation, washed with DMF and MeOH for several times and dried at 353 K in vacuu0m.

Synthesis of hybrid ZIF-67-on-CuCoBDC. Firstly, a suspension of CuBDC was prepared, the CuBDC powder was dissolved in a solution of DMF (10 ml), and stirred well at room

temperature. Then, separately preparing a metal precursor solution and a ligand solution of ZIF-67, the preparation method was slightly modified from the literature procedure. Co $(OAc)_2 \cdot 4H_2O$ was dissolved in a solution of DMF (10 mL), and 2-MeIM was dissolved in a solution of EtOH (40 mL), both the solutions were ultrasound homogenized. Finally, the CuBDC suspension was mixed with the metal precursor solution of ZIF-67, and then added to the ligand solution for mixing well, the mixture was transferred into a Teflon-lined autoclave for crystallization at 393 K for 2 days. After cooling down, the resulting dark purple powders were collected by centrifuging, washed with DMF and MeOH for several times and dried at 353 K.

Synthesis of MIL-53 (Al). In a typical synthesis, $Al(NO_3)_3 \cdot 9H_2O$ was dissolved in 15 mL of water, H_2BDC was dissolved in 40 mL of DMF for 1 h. The resulting mixture was put in a 100 mL PTEF-lined stainless steel container and then kept at 220 °C. After reacting for 72 h, the resulting white solid was filtrated, rinsed with deionized water and dried at 373 K in vacuum.

Synthesis of MIL-53 (Fe). In a typical synthesis, $Fe(NO_3)_3 \cdot 9H_2O$ and H_2BDC were added into 50 mL DMF. When the mixture became homogeneous, it was placed into an autoclave and heated at 150 °C for 24 h. After the reaction, the solution was centrifuged to collect the resultant precipitates and purified with DMF and ethanol and dried at 353 K in vacuum.

Synthesis of UiO-66. In a typical synthesis, $ZrCl_4$ and H_2BDC were dissolved in DMF (50 mL), then the solution was transferred into a 100 mL Teflon-lined stainless steel autoclave. The autoclave was sealed and heated in an oven at 120 °C for 24 h. After cooled naturally, the sample was purified with anhydrous methanol for several times to make sure that the occluded DMF molecules were eliminated, followed by drying under vacuum (100 °C, 12 h), the final UiO-66 sample was obtained.

Synthesis of other hybrid MOF-on-MOF. The synthesis method of other MOF-on-MOF hybrid materials is similar to the preparation method of ZIF-67-on-CuCoBDC, except that the MOF template is replaced from CuBDC to MIL-53 (Al), MIL-53 (Fe) and UiO-66(Zr), respectively.

Synthesis of Co_3O_4-$CuCo_2O_4$ microflowers. ZIF-67-on-CuCoBDC powders were heated to 300℃ at a rate of 5℃/min under an air atmosphere. The black product Co_3O_4-$CuCo_2O_4$ was obtained. Other derivatives were similar to the synthesis of Co_3O_4-$CuCo_2O_4$.

1.3 Characterization

The surface morphology of the prepared samples was evaluated by scanning electron microscopy (SEM, TM-1000, Hitachi, Japan) and transmission electron microscopy (TEM, JEM-1200EX, Hitachi, Japan). The change of the chemical structure was analyzed by FTIR spectroscopy (Nicolet 6700, Thermo Scientific Co., USA). Powder X-ray diffraction (XRD) data were recorded on a PNAlytical X'Pert PRO X-ray diffractometer, using Cu Kα X-rays at a scanning rate of 10° min^{-1} between 5° and 80°. Energy dispersive spectroscopy (EDS, S-3700N, Hitachi, Japan) was taken for the composition detection of different samples. The X-ray photoelectron spectroscopy (XPS) experiments were carried out on a RBD upgraded PHI-5000C ESCA system (Perkin Elmer) with Mg K radiation (h=1253.6eV), and binding energies were calibrated by using the containment carbon (C1s=284.6eV). The compositional analysis of catalysts was performed by ICP-AES in an Optima 2000 instrument (PerkinElmer, USA) after the samples calcined in an air atmosphere. The specific surface areas and pore size distribution of the samples were determined using Brunauer-Emmett-Teller (BET) and Barrett-Joyner-Halenda (BJH) analysis at a Micromeritics instrument (ASAP 2020). Thermal gravimetric (TG) was conducted on NETZSCH

STA 449 C with nitrogen and air atmosphere, respectively. H_2-temperature programmed reduction (H_2-TPR) and oxygen temperature programmed desorption (O_2-TPD) were performed on a chemical adsorption apparatus (DS-7000, HunanHuaSi) with H_2/He mixture (4% H_2 in He, 30 mL/min) as a reducing gas and the pure He as pretreatment gas at 200 ℃ for 60 min.

1.4 Catalytic experiments

In the experiment, the catalytic oxidation performance of the catalysts was measured on a self-made atmospheric fixed bed micro-reactor. 100 mg MOF-derived catalyst was placed in a Φ8×1 mm quartz reactor, a mixed gas (1 vol. % CO, 1 vol. % O_2, 98 vol. % N_2) was introduced at a flow rate of 60 ml/min. The temperature is programmed by a tubular resistance furnace, and the outlet tail gas flow is connected to a gas chromatograph (GC 1690) for online analysis via a six-way sampling valve.

1.5 Catalysis kinetics

The formula of turnover frequencies for all samples can be calculated as following:

$$\mathrm{TOF}(s^{-1}) = \frac{PV}{RT} \times COvol\% \times conversion\% / \frac{m}{M} / t$$

where P is the pressure (Pa), V/t is the volume of reactant gases through the reactor every second (m^3/s), R is the gas constant, and T is the room temperature (K), m is mass of total catalyst (g) and M is the molar mass (g/mol)

The specific reaction rate K can be calculated assuming the ideal gas behavior as follows:

K (mol g^{-1} s^{-1}) = GHSV (mL h^{-1} g^{-1}) × 1/3600 (h s^{-1}) × 1/1000 (L mL^{-1}) × CO vol.% × conversion% × 1/22.4 (mol L^{-1}) (1)

Calculation of activation energy according to the Arrhenius equation:

$$K = A \exp(-E_a/RT) \quad (2)$$

where K is the reaction rate of CO (mol CO g^{-1} s^{-1}), A is the pre-exponential factor (s^{-1}), Ea is the apparent activation energy (kJ mol^{-1}), R is the gas constant, and T is the absolute temperature (K). Taking the natural log of both sides of the equation (2), we get:

$$\ln K = -E_a/T + \ln A \quad (3)$$

By plotting ln K versus 1000/T, the apparent activation energy E_a can be calculated from the slope as shown in the figure.

2. Results and Discussions

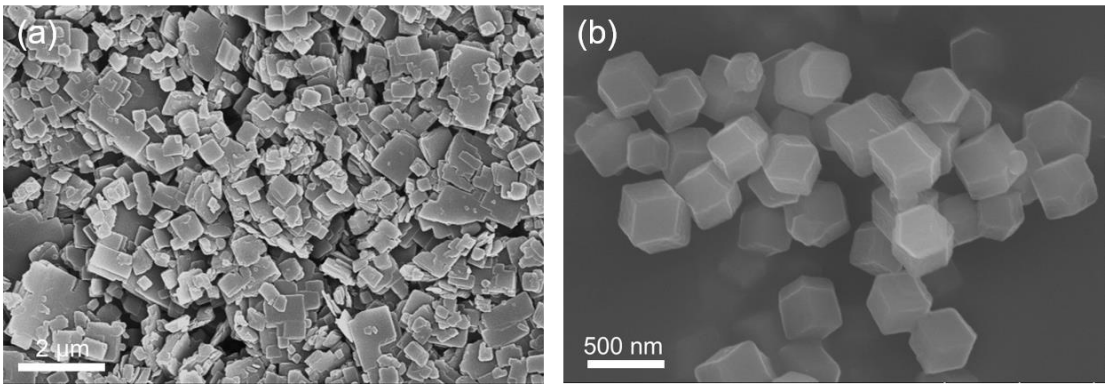

Fig. S1 SEM images of CuBDC (a), ZIF-67 (b).

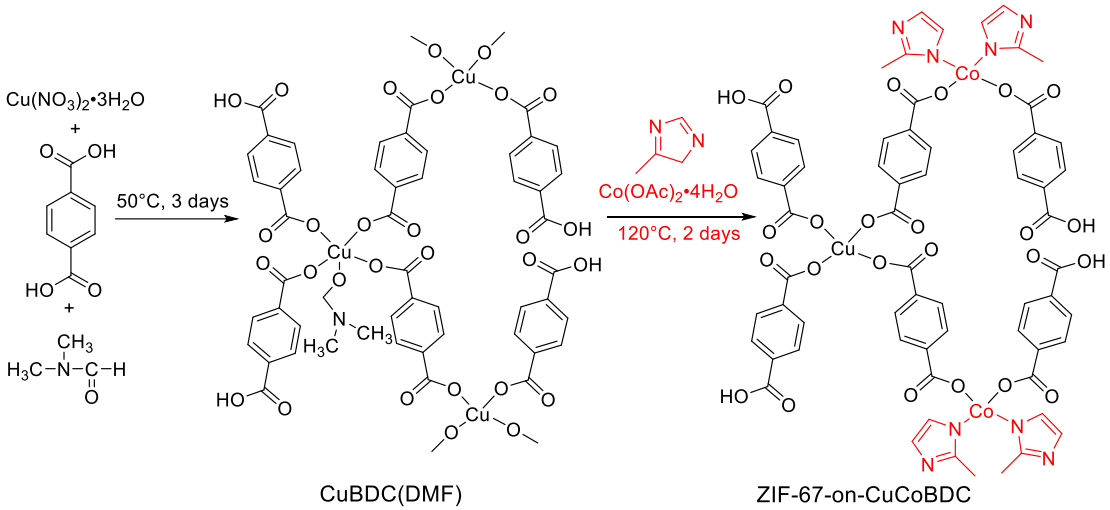

Fig. S2 The specific synthesis process of ZIF-67-on-CuCoBDC by EEGM strategy.

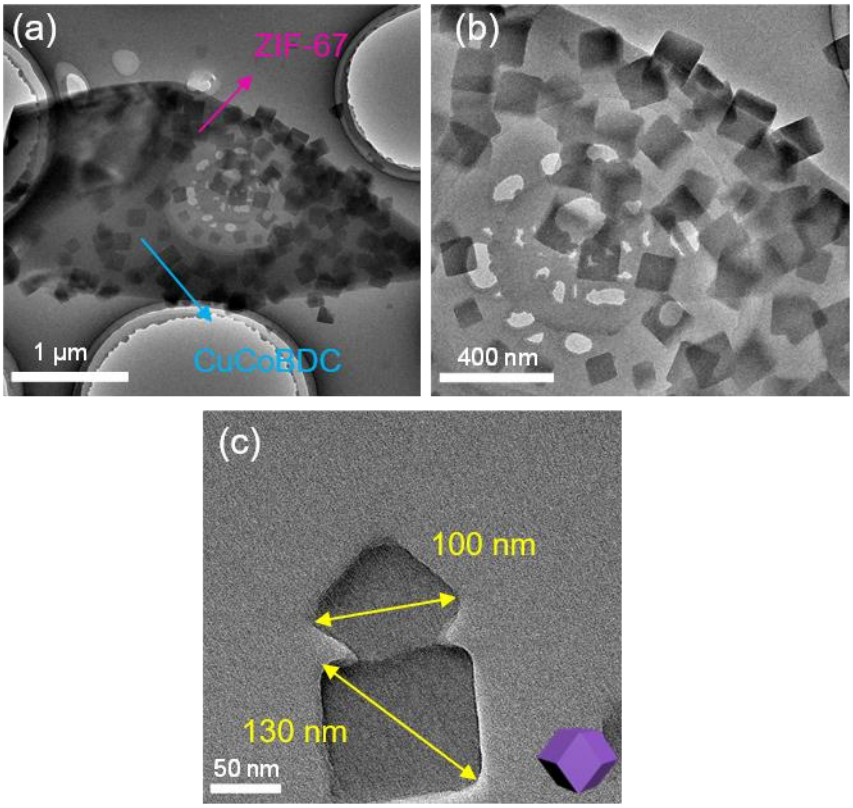

Fig. S3 TEM images of ZIF-67-on-CuCoBDC(a-c). The images showed the MOF particles after ultrasonic dispersion, it can be seen that ZIF-67-on-CuCoBDC microflowers had a stable hybrid structure, in which dodecahedral ZIF-67 nanoparticles were uniformly distributed on the surface of the CuCoBDC template with a size of about 100 nm.

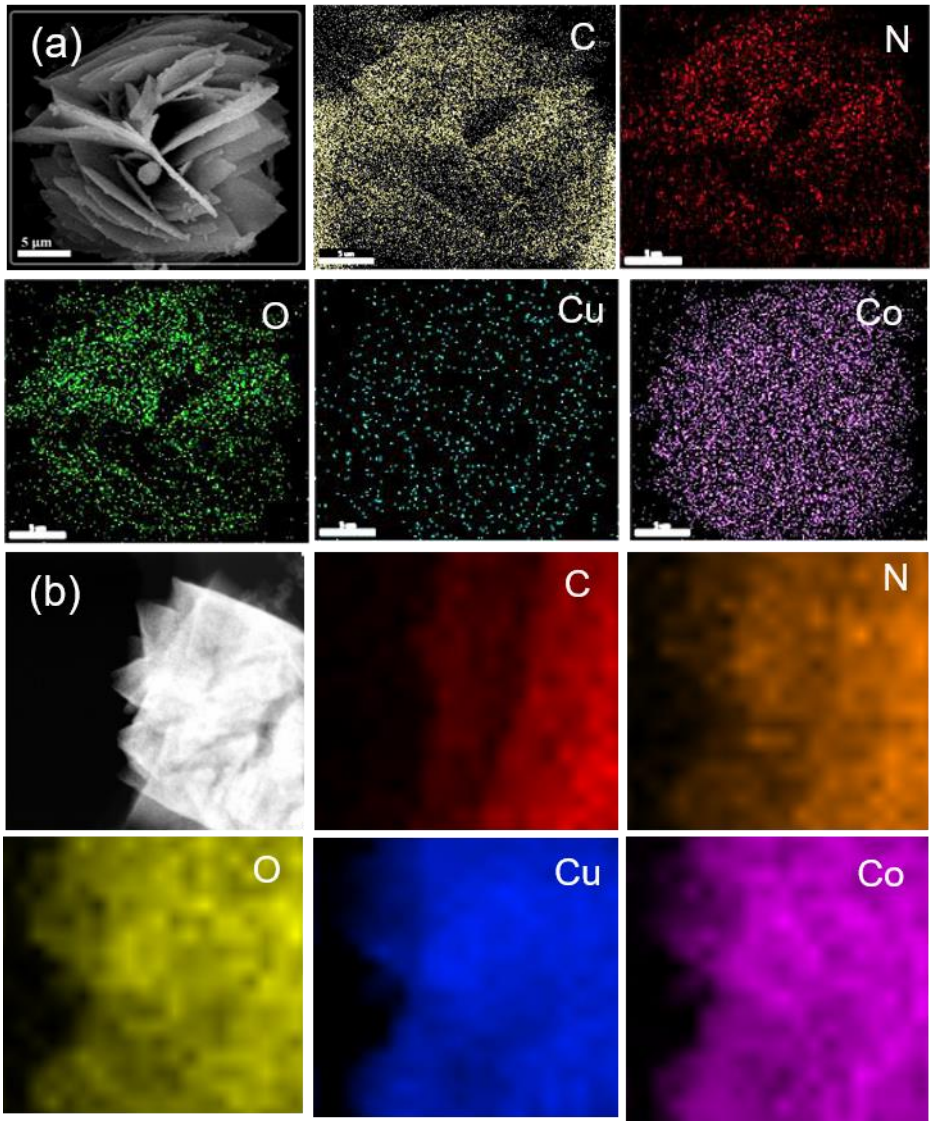

Fig. S4 Corresponding SEM-elemental mapping images of the C, N, O, Cu, Co in ZIF-67-on-CuCoBDC sample (a), Corresponding STEM-elemental mapping images of C, N, O, Cu, Co in Co_3O_4-$CuCo_2O_4$ sample (b).

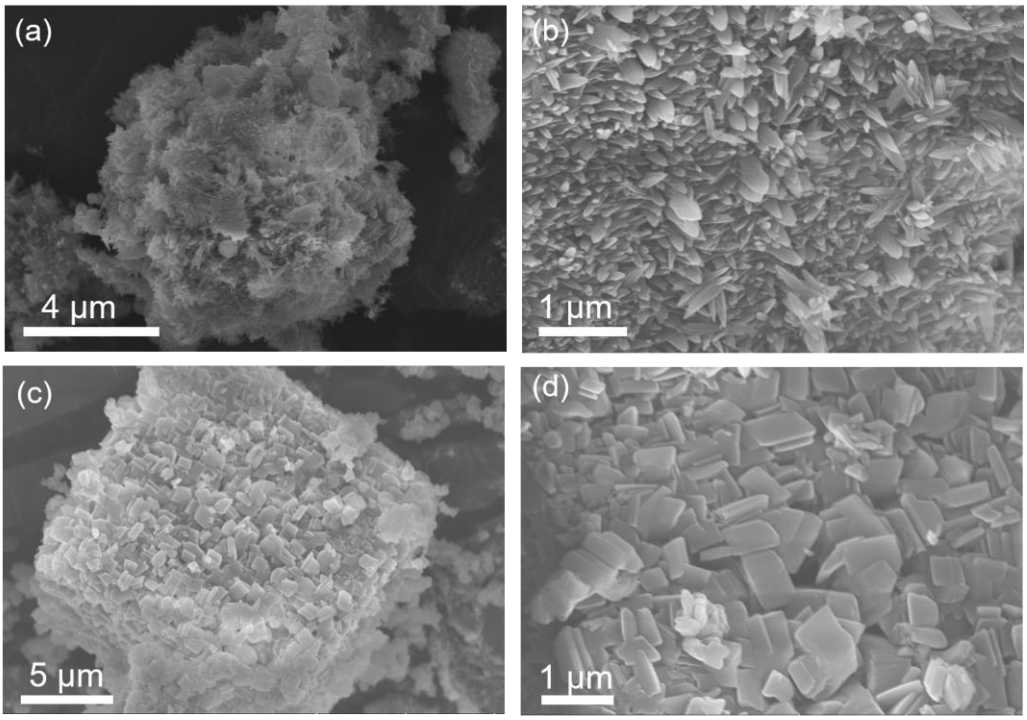

Fig. S5 SEM images of CuCoBDC (a, b) and CuBDC-MI (c, d).

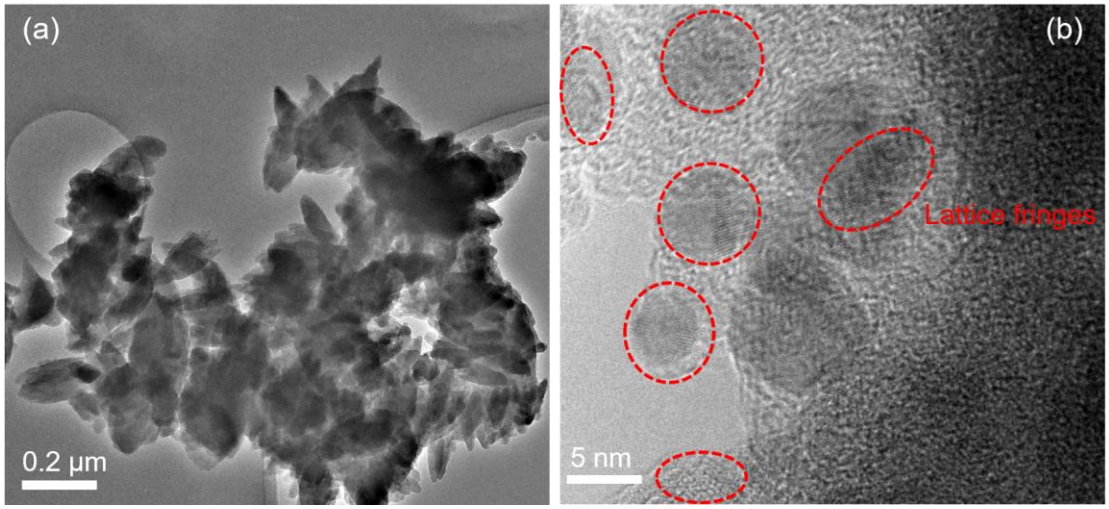

Fig. S6 TEM (a) and HRTEM (b) images of CuCoBDC.

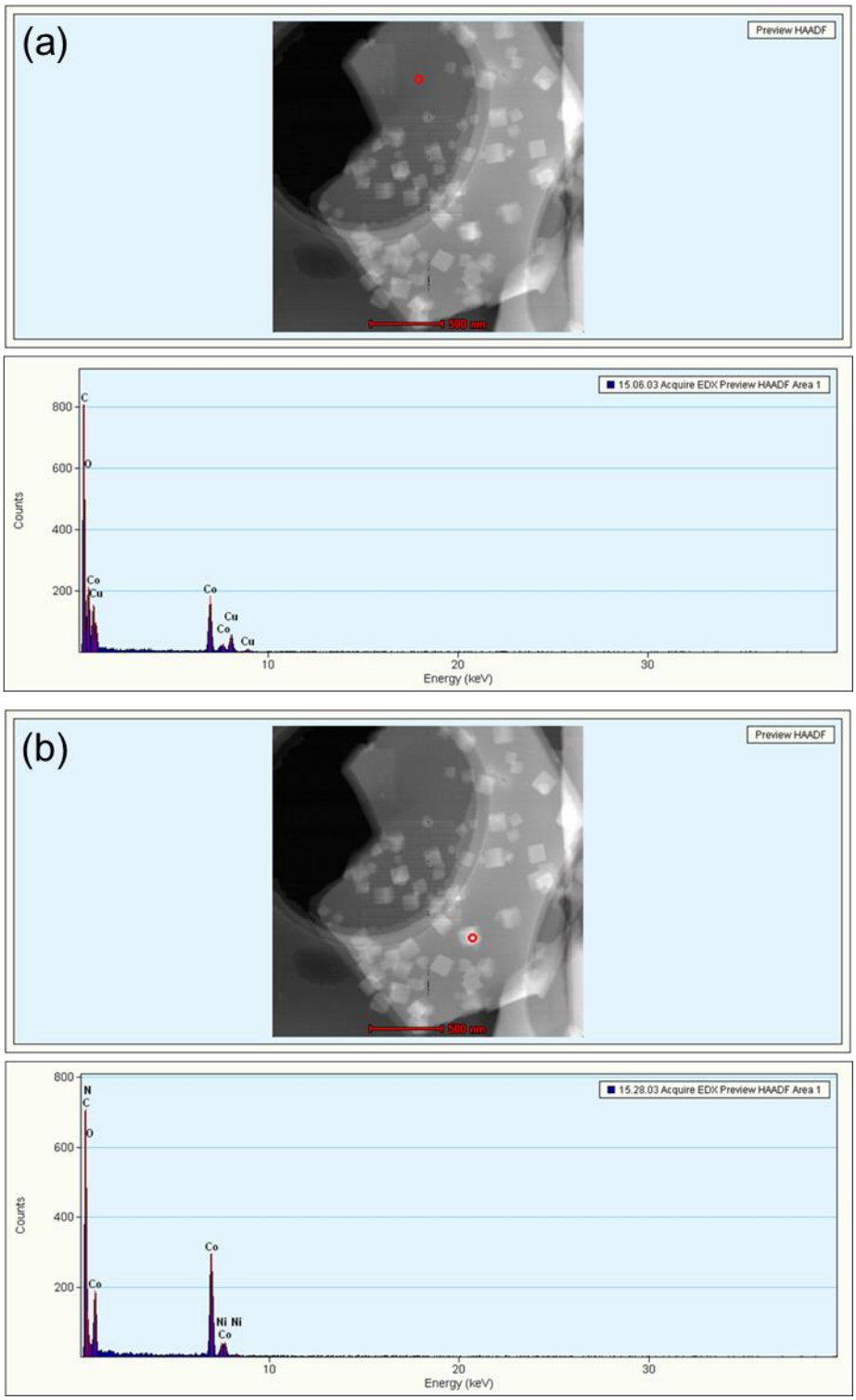

Fig. S7 EDS point scanning of ZIF-67-on-CuCoBDC materials.

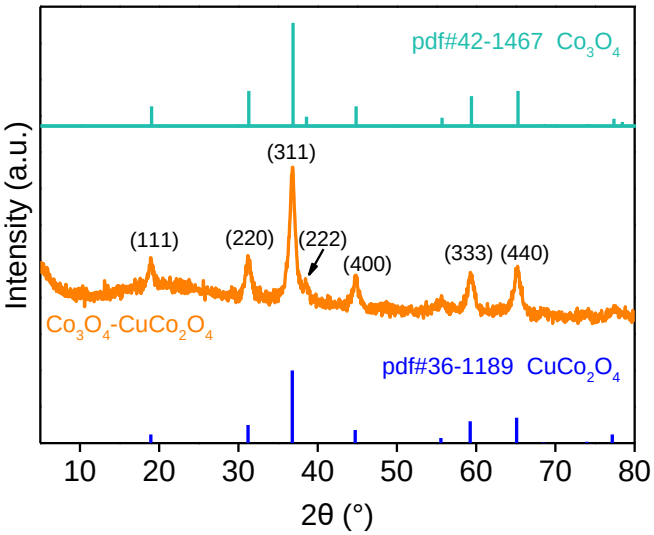

Fig. S8 XRD spectra of Co_3O_4-$CuCo_2O_4$.

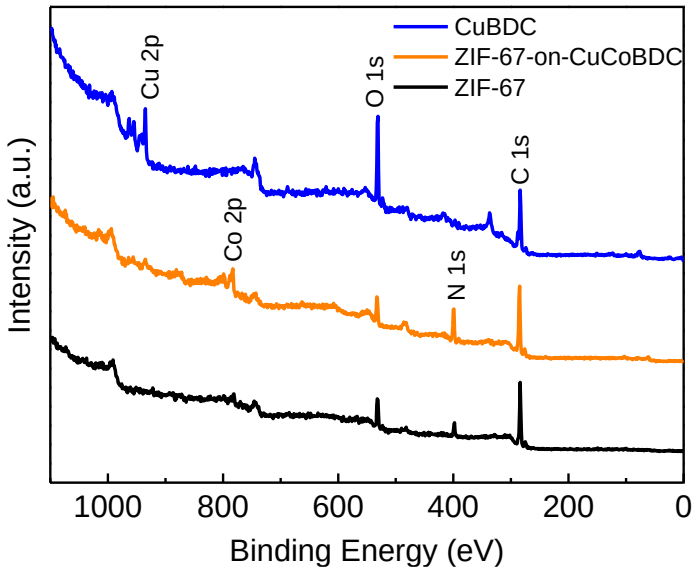

Fig. S9 XPS spectra of CuBDC, ZIF-67 and ZIF-67-on-CuCoBDC.

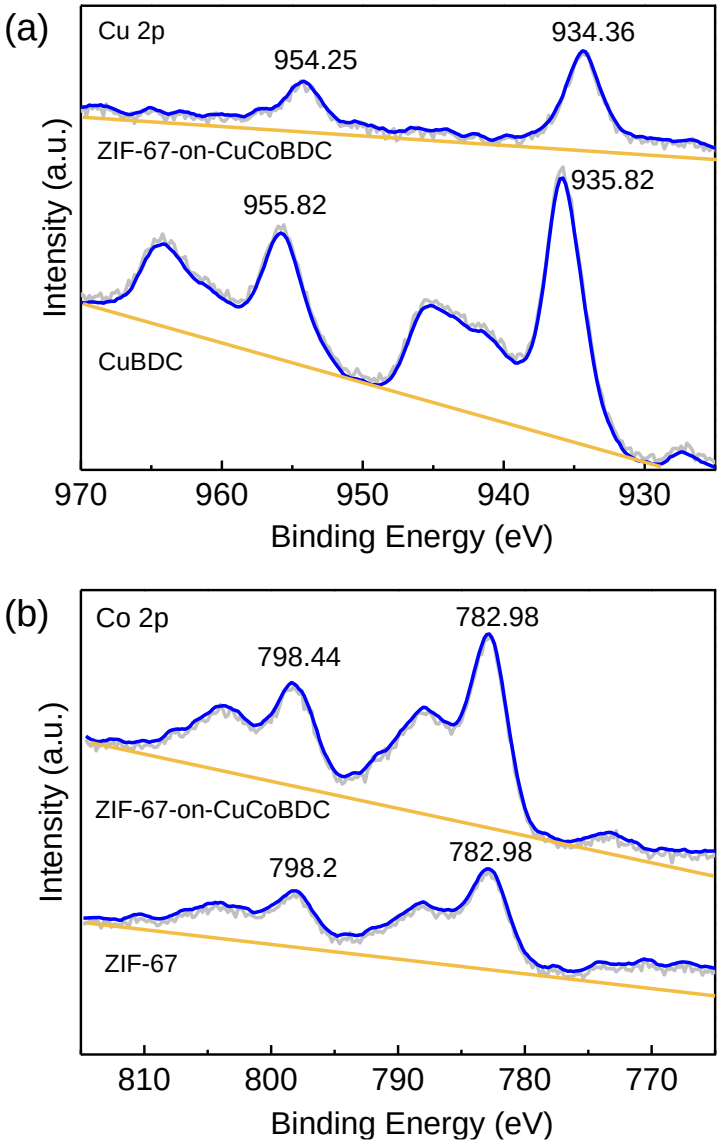

Fig. S10 XPS spectra of Cu 2p and Co 2p for ZIF-67-on-CuCoBDC.

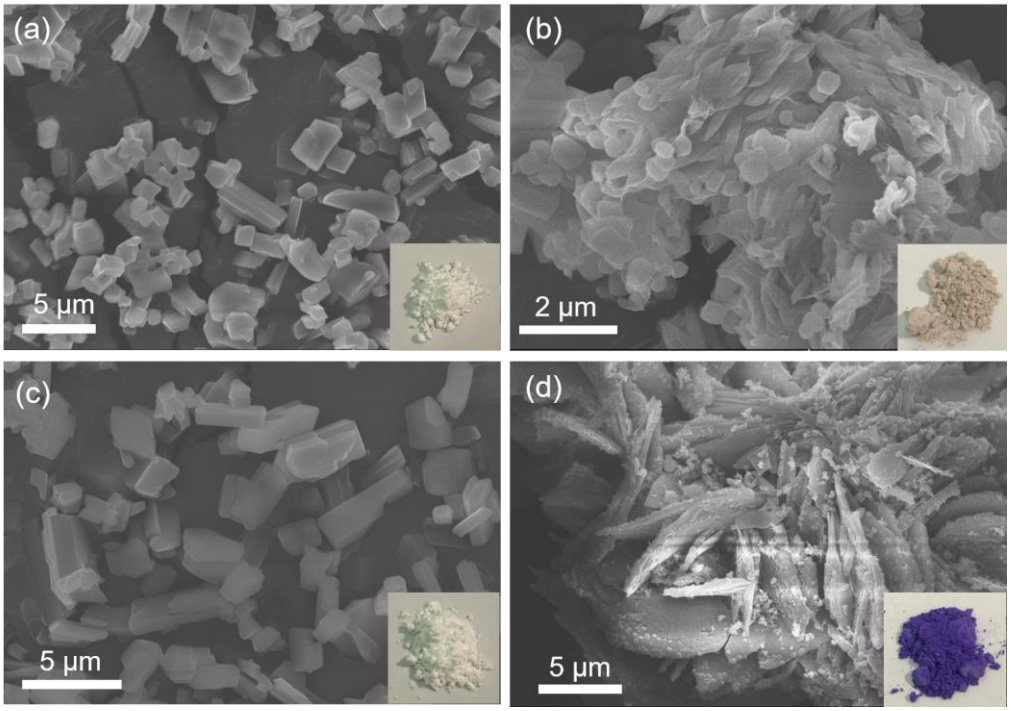

Fig. S11 SEM and actual images of MIL-53(Al) (a), MIL-53(AlCo) (b), MIL-53 (Al)+2-MI (c), ZIF-67-on- MIL-53(AlCo) (d). It was obvious that after the reaction of MIL-53(Al) with $Co(OAc)_2$, its morphology changed from the original cubic shape to the fusiform flake shape, and the color of the actual product changed significantly. However, after reacting with 2-MI, its micro- and macro-morphology remained basically unchanged. This further validates the mechanism of action of the EGGM strategy and extends its applicability to the construction of MOF-on-MOF heterostructures even on more inert MOF surfaces.

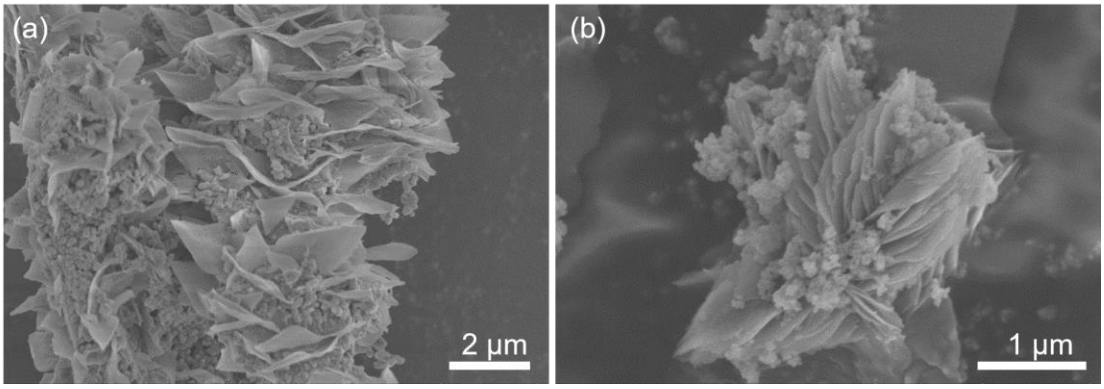

Fig. S12 SEM images of ZIF-67-on-MIL-53 (FeCo) (a), ZIF-67-on-UiO-66(ZrCo) (b).

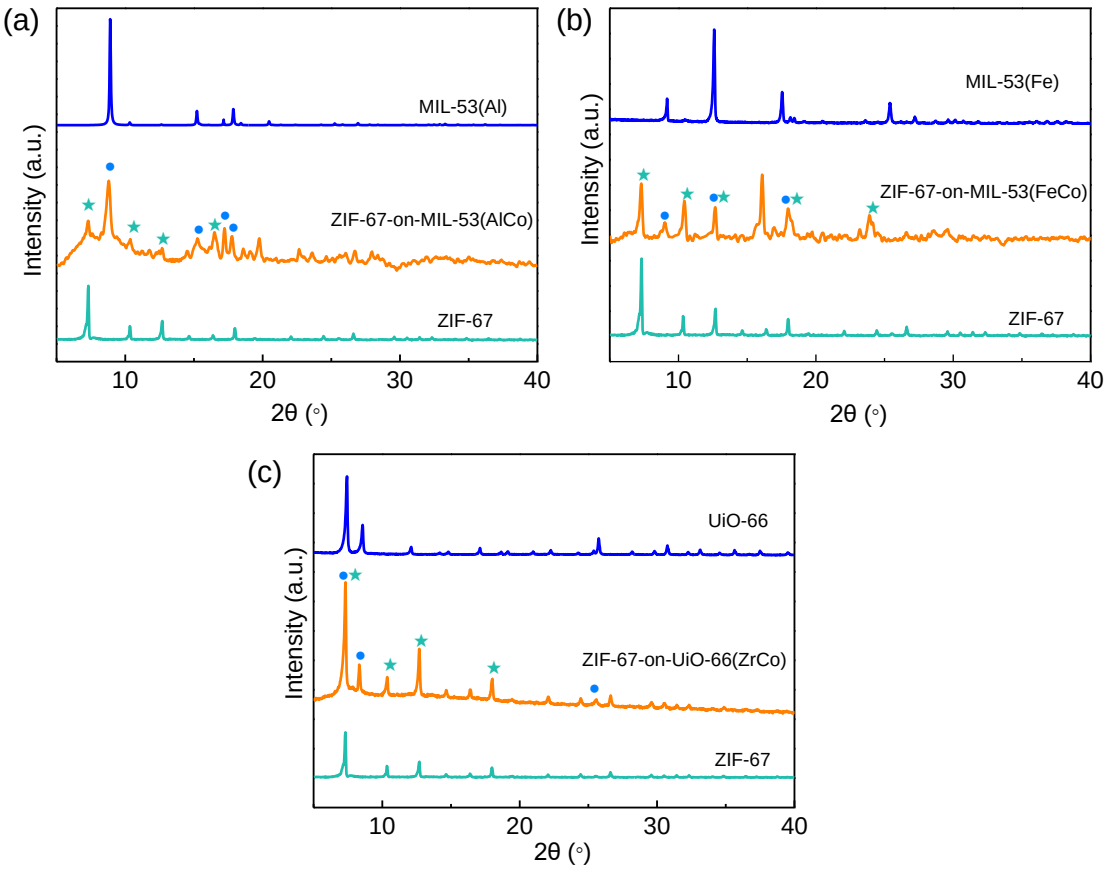

Fig. S13 XRD patterns of ZIF-67-on-MIL-53(AlCo) (a), ZIF-67-on-MIL-53(FeCo) (b) and ZIF-67-on-UiO-66(ZrCo) (c).

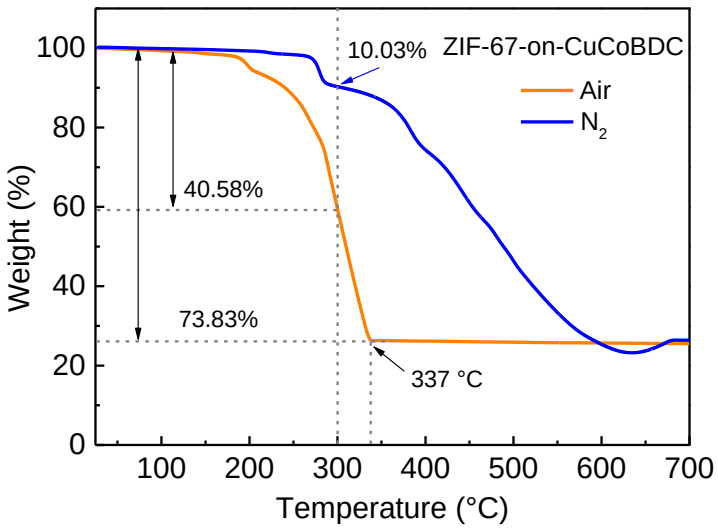

Fig. S14 Thermal gravimetric analyses of ZIF-67-on-CuCoBDC in nitrogen and air atmosphere, respectively.

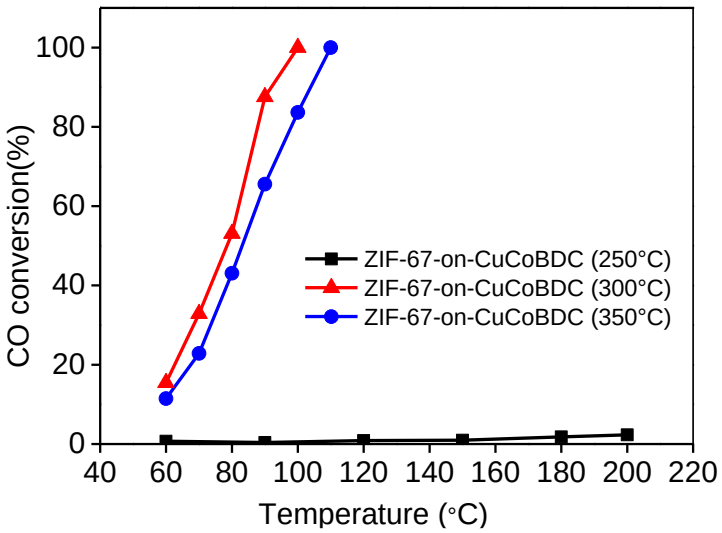

Fig. S15 Effect of calcination temperature on the catalytic activity of CuO-$CuCo_2O_4$ for CO oxidation.

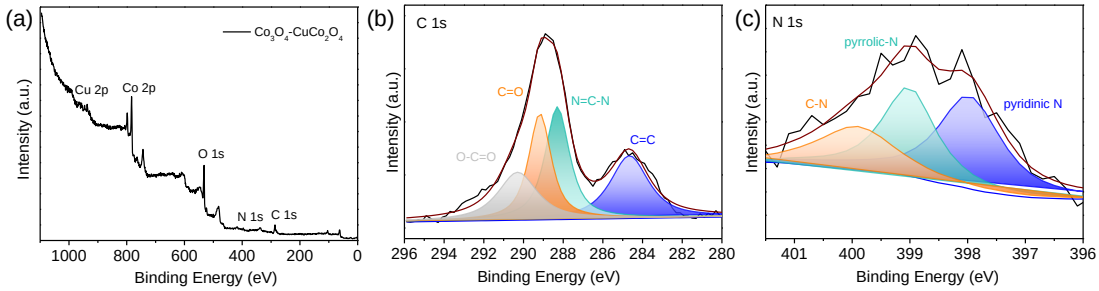

Fig. S16 XPS survey spectrum (a) and high-resolution XPS spectra of C 1s (b), N 1s (c) for Co_3O_4-$CuCo_2O_4$.

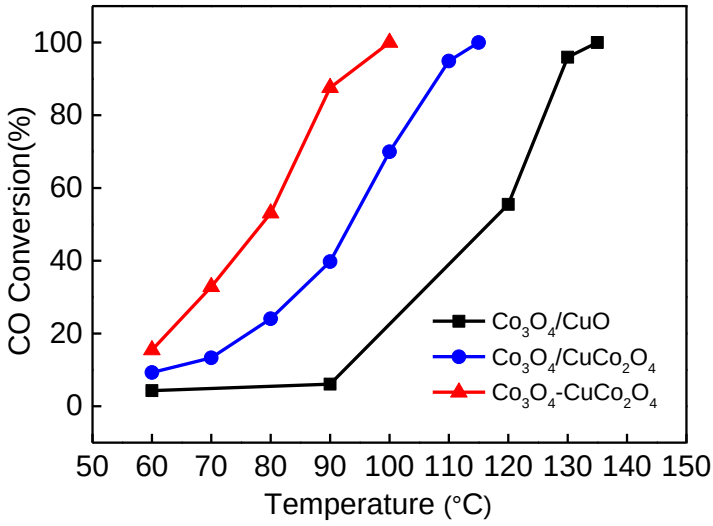

Fig. S17 CO conversion of $Co_3O_4/CuCo_2O_4$ and Co_3O_4/CuO derived from ZIF-67/CoCuBDC and ZIF-67/CuBDC precursors.

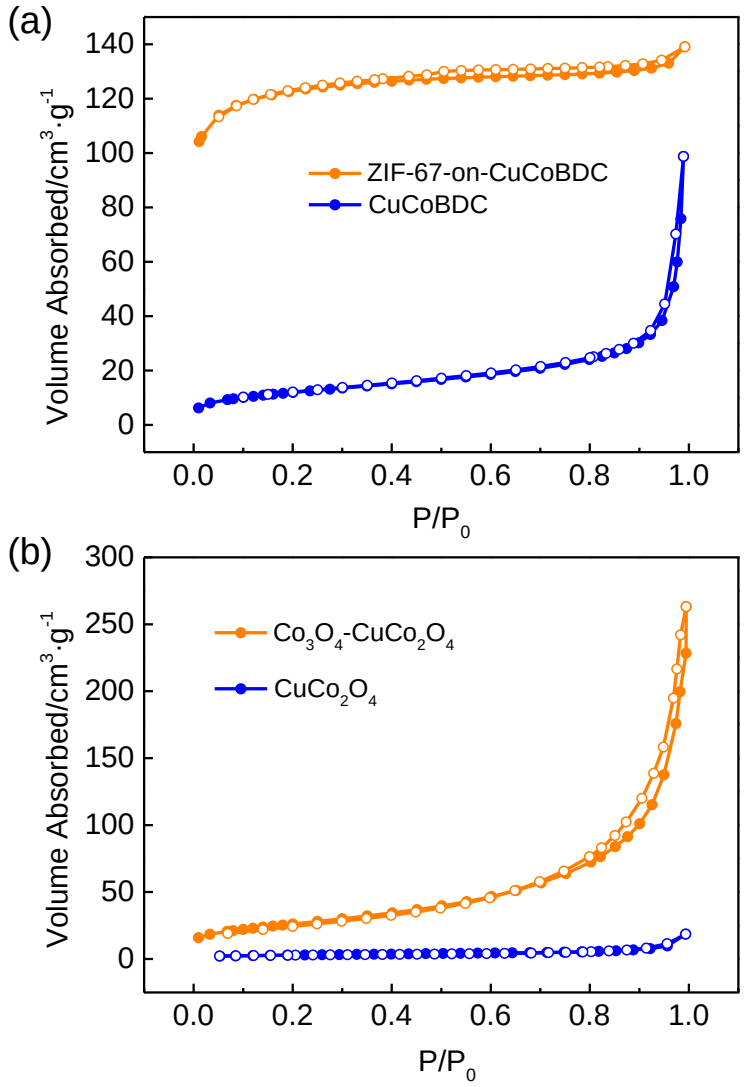

Fig. S18 N_2 adsorption-desorption isotherms of CuCoBDC and ZIF-67-on-CuCoBDC (a), $CuCo_2O_4$ and Co_3O_4-$CuCo_2O_4$(b). From the MOF precursor, the BET specific surface area of obtained CuCoBDC was only 43.77 m^2/g, after extended growth, the surface area was up to 408.11 m^2/g. More directly, the specific surface area of the hybrid Co_3O_4-$CuCo_2O_4$ catalyst was 93.85 m^2/g, which was much higher than that of the CuCoBDC derivative (10.36 m^2/g)

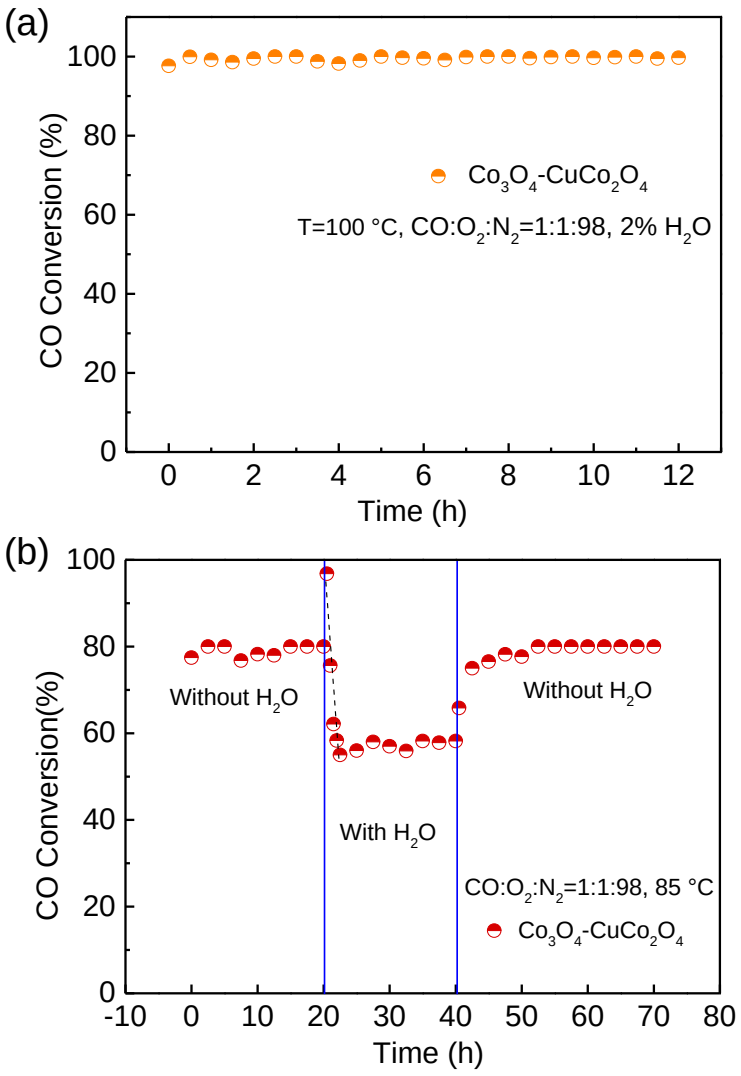

Fig. S19 Long-term durability test of as-prepared Co_3O_4-$CuCo_2O_4$ catalysts tested at 100 ℃ (a), the resistance of H_2O at 80% of CO conversion on catalyst stability tested at 85 ℃ (b).

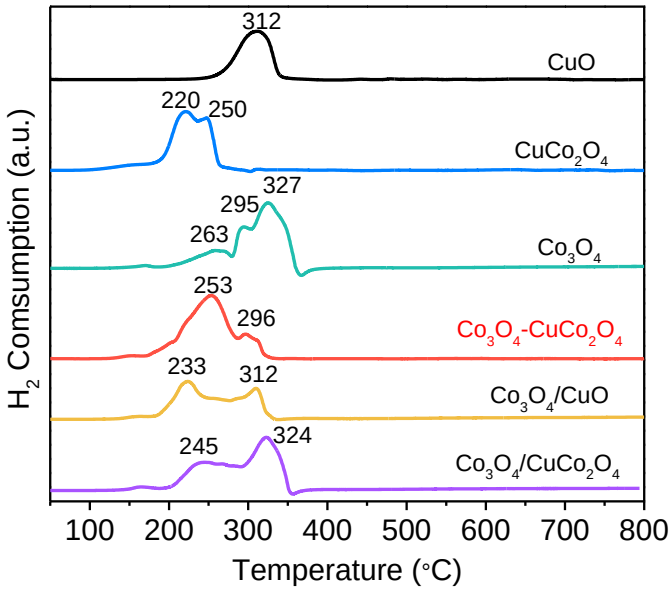

Fig. S20 H_2-TPR of profiles of the CuO, $CuCo_2O_4$, Co_3O_4, Co_3O_4-$CuCo_2O_4$, Co_3O_4/CuO, and Co_3O_4/$CuCo_2O_4$ derived from CuBDC, CuCoBDC, ZIF-67, ZIF-67-on-CuCoBDC, ZIF-67/CuBDC and ZIF-67/CuCoBDC.

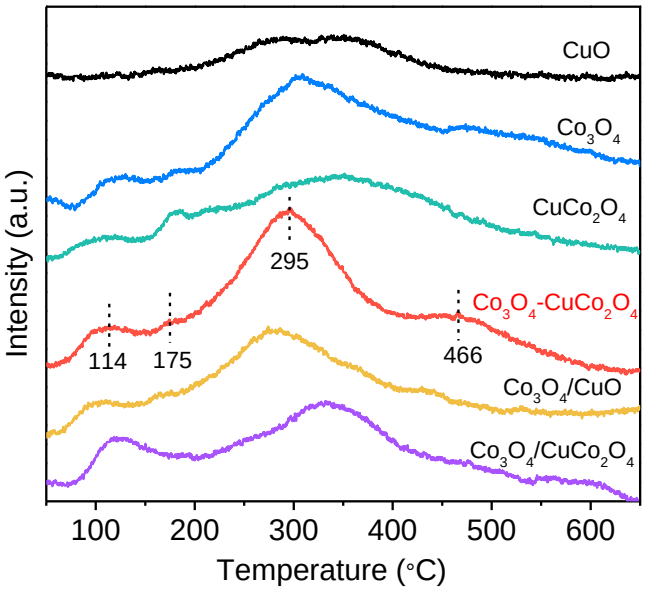

Fig. S21 O_2-TPD of profiles of the CuO, $CuCo_2O_4$, Co_3O_4, Co_3O_4-$CuCo_2O_4$, Co_3O_4/CuO, and Co_3O_4/$CuCo_2O_4$ derived from CuBDC, CuCoBDC, ZIF-67, ZIF-67-on-CuCoBDC, ZIF-67/CuBDC and ZIF-67/CuCoBDC.